Available online at www.sciencedirect.com
ScienceDirect
International Journal of Thermal Sciences 48 (2009) 475–487
International Journal of Thermal Sciences
www.elsevier.com/locate/ijts

# Thermal management of a symmetrically heated channel–chimney system

Assunta Andreozzi [a,*], Bernardo Buonomo [b], Oronzio Manca [b]

[a] *Dipartimento di Energetica, Termofluidodinamica applicata e Condizionamenti ambientali, Università degli Studi di Napoli Federico II, Piazzale Tecchio 80, 80125 Napoli, Italy*

[b] *Dipartimento di Ingegneria Aerospaziale e Meccanica, Seconda Università degli Studi di Napoli, Via Roma 29, 81031 Aversa (CE), Italy*

Received 25 July 2007; received in revised form 20 March 2008; accepted 21 March 2008

Available online 24 April 2008

**Abstract**

A parametric analysis of natural convection in air, in a channel–chimney system, symmetrically heated at uniform heat flux, obtained by means of a numerical simulation, is carried out. The analyzed regime is two-dimensional, laminar and steady-state. Results are presented in terms of wall temperature profiles in order to show the more thermally convenient configurations which correspond to the channel–chimney system with the lowest maximum wall temperature. For the considered Rayleigh number, the difference between the highest and the lowest maximum wall temperatures increases with increasing the channel aspect ratio. The optimal expansion ratio values depend strongly on the Rayleigh number and extension ratio values and slightly on the channel aspect ratio. Correlations for dimensionless mass flow rate, maximum wall temperature and average Nusselt number, in terms of Rayleigh number and dimensionless geometric parameters are presented in the ranges: $5 \leqslant Ra^* \leqslant 2.0 \times 10^4$, $1.5 \leqslant L/L_h \leqslant 4.0$ and $1.0 \leqslant B/b \leqslant 4.0$.



*Keywords:* Thermal management; Natural convection; Vertical channel–chimney system; Thermal optimization; Thermal design

## 1. Introduction

Natural convection between heated vertical parallel plates, due to its several engineering applications, such as thermal control in electronic equipments, nuclear reactors, solar collectors and chemical vapor deposition reactors, has been extensively studied both experimentally and numerically [1–3]. More recent trends in natural convection research are to find new configurations to improve the heat transfer parameters or to analyze standard configurations to carry out optimal geometrical parameters for a better heat transfer rate [3–10]. A particularly interesting geometry of modified channel configurations is obtained by placing of adiabatic extensions downstream of the heated channel, the channel–chimney system.

As shown in [8], some optimal configurations of this system can enhance the heat transfer up to 20% and reduce the maximum wall temperature significantly. The optimal configurations depend on the dimensionless geometrical parameters, such as the expansion ratio (the distance between the adiabatic extensions, $B$, over the distance between the heated plates, $b$), the extension ratio (the total length of the channel–chimney system, $L$, over the channel length, $L_h$), the channel aspect ratio (the channel length, $L_h$, over the channel gap $b$) and the Rayleigh number. A parametric analysis of the channel–chimney system is necessary in order to carry out a correct thermal management of this configuration. In fact, an in-depth study allows to evaluate the optimal configurations and to avoid geometrical parameter values which determine a reduction of the chimney effect due to a cold inflow in the system from the outlet section of the adiabatic extensions.

In the following, a short review on the channel–chimney system is given. The chimney effect, due to a parallel-wall adiabatic channel, with heat sources at the channel inlet was studied for the first time in [11]. The channel with straight adiabatic downstream extensions was numerically investigated in [12–14]. A vertical channel with isothermal parallel walls was analyzed for natural convection in air in [12]. A vertical

* Corresponding author. Tel.: +39 0817682645; fax: +39 081 2390364.
*E-mail address:* assunta.andreozzi@unina.it (A. Andreozzi).

1290-0729/$ – see front matter 
doi:10.1016/j.ijthermalsci.2008.03.017

**Nomenclature**

| | | |
|---|---|---|
| $a$ | thermal diffusivity | $m^2/s$ |
| $b$ | channel gap | m |
| $B$ | chimney gap | m |
| $g$ | acceleration due to the gravity | $m/s^2$ |
| $Gr$ | Grashof number, Eq. (5) | |
| $h(x)$ | local convective coefficient | $W/m^2\,K$ |
| $k$ | thermal conductivity | $W/m\,K$ |
| $L$ | channel–chimney height | m |
| $L_h$ | channel height | m |
| $L_x$ | height of the reservoir | m |
| $L_y$ | width of the reservoir | m |
| $n_x$ | number of nodes along $x$-direction | |
| $n_y$ | number of nodes along $y$-direction | |
| $Nu(X)$ | local Nusselt number, Eq. (6) | |
| $Nu$ | average Nusselt number, Eq. (7) | |
| $p$ | pressure | Pa |
| $P$ | dimensionless pressure, Eq. (5) | |
| $Pr$ | Prandtl number, Eq. (5) | |
| $\dot{q}$ | heat flux | $W/m^2$ |
| $Ra$ | Rayleigh number, Eq. (5) | |
| $Ra^*$ | channel Rayleigh number, Eq. (5) | |
| $T$ | temperature | K |
| $u, v$ | velocity components along $x$, $y$ | m/s |
| $U, V$ | dimensionless velocity components, Eq. (5) | |
| $x, y$ | Cartesian coordinates | m |
| $X, Y$ | dimensionless coordinates, Eq. (5) | |

*Greek symbols*

| | | |
|---|---|---|
| $\beta$ | coefficient of volumetric expansion, $1/K$ | |
| $\Delta\Psi$ | mass flow rate | |
| $\theta$ | dimensionless temperature, Eq. (5) | |
| $\nu$ | kinematic viscosity | $m^2/s$ |
| $\psi$ | stream function | $m^2/s$ |
| $\Psi$ | dimensionless stream function, Eq. (5) | |
| $\rho$ | density | $kg/m^3$ |
| $\omega$ | vorticity | $1/s$ |
| $\Omega$ | dimensionless vorticity, Eq. (5) | |

*Subscripts*

| | |
|---|---|
| 0 | simple channel |
| $\infty$ | free stream condition |
| max | maximum value |
| opt | optimal value |
| $w$ | channel wall |
| $w_1$ | left channel wall |
| $w_2$ | right channel wall |

isothermal or isoflux channel with unheated extensions located upstream or downstream of the channel was studied in [13,14].

The effect of expansion ratio greater than 1.0 with symmetrically heated channel or heated tube was investigated in [8,15–19]. A system with symmetrically heated channel at uniform wall heat flux was studied experimentally in [8,17] and numerically in [18]. Local temperature measurements of the air flow in the channel and the chimney were carried out in [17] and different fluid motion regions were detected inside the chimney. A numerical simulation of natural convection in air, in a channel–chimney system, heated symmetrically at uniform heat flux was carried out in [18]. The comparison with experimental data, given in [8], provided some differences although thermal and dynamic behaviors were the same. Results explained that the cold inflow at the outlet section worsened the chimney effect. A periodic isothermal vertical channel expanded-chimney was examined in [19]. Each sub-system channel–chimney was the same as the analyzed configuration in [16]. For the channel–chimney system with asymmetrical heating, two experimental investigations were carried out [20,21]. Thermal design procedure of symmetrically and asymmetrically heated channel–chimney systems in air was proposed in [22]. The design charts for the evaluation of thermal parameters were accomplished, elaborating experimental data and correlations given in [8,20].

As analyzed in [10], the present study is also conceived as an attempt to estimate the right balance between the control of the maximum wall temperature and an applied symmetrical wall heat flux. Moreover, this can also be viewed as the maximization of heat transfer density for an assigned volume that is constrained by space limitations. The first objective can be attained by a channel–chimney system that resembles the one analyzed in [18]. The second objective has been studied by Bejan and coauthors [4,9,23,24], and as of late it has been reviewed in [25].

A new concept for generating the multi-scale structure of a finite size flow system which has maximum heat transfer density, maximum heat transfer in a fixed volume, was presented in [23]. They maximize the heat transfer density in laminar forced convection in parallel isothermal blades by constructal theory [4] optimizing the spacing between adjacent blades of progressively smaller scales. This theory was applied in [24] to obtain multi-scale structures in natural convection in order to maximize the heat transfer density. The flow volume was filled with vertical equidistant heated blades of decreasing lengths. A numerical study was carried out to compare the results of the global analysis. The geometric optimization of L- and C-shaped channels in laminar natural convection with the objective to maximize the heat transfer in the channel was accomplished in [9].

In this paper, a parametric analysis of natural convection in air, in a channel–chimney system symmetrically heated at uniform heat flux, obtained by means of a numerical simulation, is carried out. The analyzed regime is two-dimensional, laminar and steady-state. The geometry studied in this numerical investigation is important in different technical fields, such as in electronic cooling [5–10,16–22] and in building and houses solar components, as indicated in [9,26,27]. It has to be remarked that the evaluation of the mass flow rate in the experimental in-

vestigation in natural convection is not easy. Then, by means of a numerical procedure, it is simpler to give this information also in terms of correlation as a function of the Rayleigh number and dimensionless geometrical parameters. It seems that this is not available in open literature about the channel–chimney systems [8,16,18,19,22]. The present investigation enlarges the results given in [18] taking into account the effect of the channel aspect ratio on the natural convective heat transfer parameters in channel–chimney systems. Moreover, the optimal value of expansion ratio corresponding to the highest average Nusselt number and dimensionless mass flow rate and the lowest dimensionless maximum wall temperature are evaluated and a correlation in terms of Rayleigh number and extension ratio is proposed. These information extend the results of the experimental investigation [8] and the thermal design procedure [22]. Results are presented in terms of wall temperature profiles in order to show the more thermally convenient configurations which correspond to the channel–chimney system with the lowest maximum wall temperature. Geometric optimal configurations, for assigned Rayleigh number and aspect ratio, are estimated as a function of the extension ratio. For these optimal configurations, the global thermal and fluid dynamic behaviors are evaluated and correlated as a function of the extension ratio. The analysis is obtained for different Rayleigh numbers, channel aspect ratios and extension and expansion ratios. Correlations for dimensionless mass flow rate, maximum wall temperature and average Nusselt number in terms of Rayleigh number, channel aspect ratio, extension and expansion ratios are presented in the ranges: $5 \leqslant Ra^* \leqslant 2.0 \times 10^4$, $1.5 \leqslant L/L_h \leqslant 4.0$ and $1.0 \leqslant B/b \leqslant 4.0$.

## 2. Problem formulation

The aim of this paper is the numerical analysis of natural convection in air in a symmetrically heated vertical channel, considering the presence of two downstream adiabatic extensions to enhance the "chimney effect". In the following, the heated part is indicated as channel and the unheated part as chimney. The investigated geometry is depicted in Fig. 1(a).

It is made up of a vertical channel with two parallel plates, heated at uniform heat flux $\dot{q}$; the height of the channel plates is $L_h$ whereas the distance between them is $b$. On the top of the channel, there is a chimney made of two insulated parallel and vertical plates; their height is $(L - L_h)$ and the distance between them is $B$. An enlarged computational domain has been chosen. It is made up of the geometry described previously and of two reservoirs of height $L_x$ and width $L_y$, which are placed upstream of the channel and downstream of the chimney. The reservoirs are important because they simulate the thermal and fluid dynamic behaviors far away the inflow and outflow regions. The employed computational domain is shown in Fig. 1(b); in this figure the solid lines and the dotted lines indicate the walls and the open-boundaries, respectively.

The governing equations, in terms of stream-function and vorticity, which are defined as:

$$u = \frac{\partial \psi}{\partial y}; \qquad v = -\frac{\partial \psi}{\partial x}; \qquad \omega = \frac{\partial v}{\partial x} - \frac{\partial u}{\partial y} \tag{1}$$

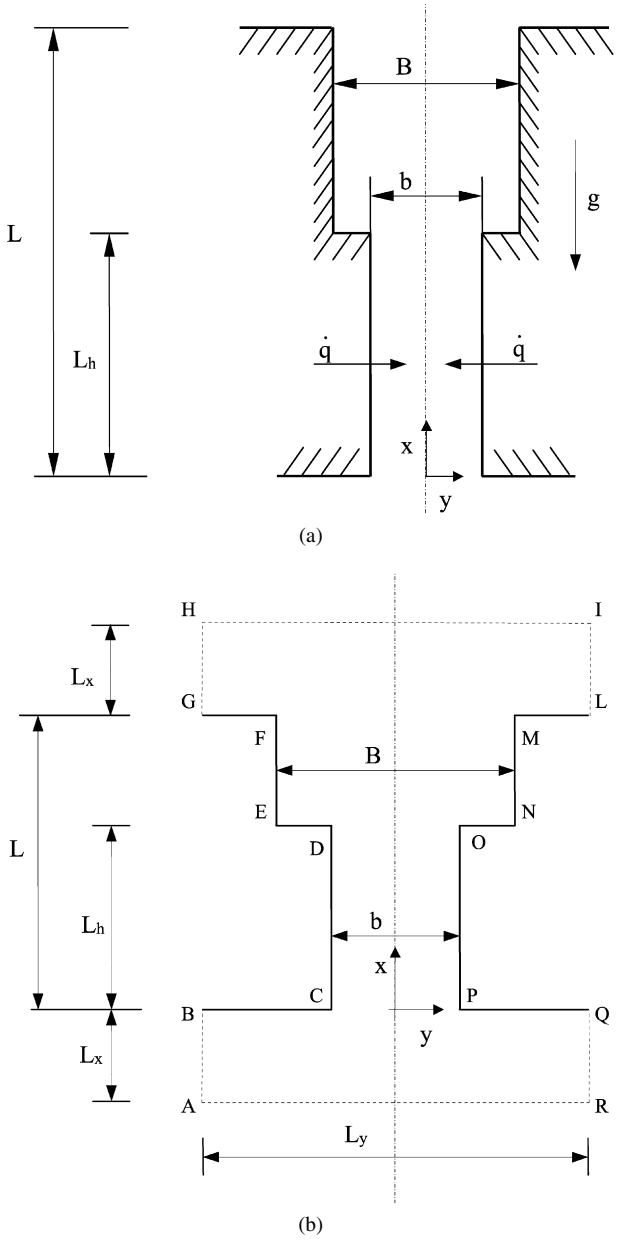


Fig. 1. Geometry of the problem: (a) Physical configuration, (b) Computational domain.

are, in dimensionless form:

$$\frac{\partial (U\Omega)}{\partial X} + \frac{\partial (V\Omega)}{\partial Y} = \frac{\partial^2 \Omega}{\partial X^2} + \frac{\partial^2 \Omega}{\partial Y^2} - Gr\frac{\partial \theta}{\partial Y} \tag{2}$$

$$\frac{\partial^2 \Psi}{\partial X^2} + \frac{\partial^2 \Psi}{\partial Y^2} = -\Omega \tag{3}$$

$$\frac{\partial (U\theta)}{\partial X} + \frac{\partial (V\theta)}{\partial Y} = \frac{1}{Pr}\left(\frac{\partial^2 \theta}{\partial X^2} + \frac{\partial^2 \theta}{\partial Y^2}\right) \tag{4}$$

where the dissipative term and that involving the material derivative of the pressure were neglected, according to [1]. Eqs. (2)–(4) were derived under the hypotheses of laminar, two-dimensional flow, steady-state regime and taking the thermophysical properties to be constant with temperature except for the density, as suggested by the Boussinesq approximation.

Table 1
Boundary conditions

| $\Psi$ | $\Omega$ | $\theta$ | Zone |
|---|---|---|---|
| $\frac{\partial^2\Psi}{\partial X^2}=0$ | $\frac{\partial\Omega}{\partial X}=0$ | $\theta=0$ | AR |
| $\frac{\partial^2\Psi}{\partial Y^2}=0$ | $\frac{\partial\Omega}{\partial Y}=0$ | $\theta=0$ | AB and QR |
| $\Psi=\Psi_{w1}$ | $\frac{\partial\Psi}{\partial X}=0$ | $\frac{\partial\theta}{\partial X}=0$ | BC, DE and FG |
| $\Psi=\Psi_{w2}$ | $\frac{\partial\Psi}{\partial X}=0$ | $\frac{\partial\theta}{\partial X}=0$ | PQ, NO and LM |
| $\Psi=\Psi_{w1}$ | $\frac{\partial\Psi}{\partial Y}=0$ | $\frac{\partial\theta}{\partial Y}=-1$ | CD |
| $\Psi=\Psi_{w2}$ | $\frac{\partial\Psi}{\partial Y}=0$ | $\frac{\partial\theta}{\partial Y}=1$ | OP |
| $\Psi=\Psi_{w1}$ | $\frac{\partial\Psi}{\partial Y}=0$ | $\frac{\partial\theta}{\partial Y}=0$ | EF |
| $\Psi=\Psi_{w2}$ | $\frac{\partial\Psi}{\partial Y}=0$ | $\frac{\partial\theta}{\partial Y}=0$ | MN |
| $\frac{\partial^2\Psi}{\partial Y^2}=0$ | $\frac{\partial\Omega}{\partial Y}=0$ | $\frac{\partial\theta}{\partial Y}=0$ | GH and IL |
| $\frac{\partial^2\Psi}{\partial X^2}=0$ | $\frac{\partial\Omega}{\partial X}=0$ | $\frac{\partial\theta}{\partial X}=0$ | HI |

The employed dimensionless variables are:

$$X=\frac{x}{b},\qquad Y=\frac{y}{b},\qquad U=\frac{ub}{\nu}$$
$$V=\frac{vb}{\nu},\qquad P=\frac{(p-p_\infty)b^2}{\rho\nu^2}$$
$$\theta=\frac{(T-T_\infty)k}{\dot{q}b},\qquad \Psi=\frac{\psi}{\nu},\qquad \Omega=\frac{\omega b^2}{\nu}$$
$$Gr=\frac{g\beta\dot{q}b^4}{k\nu^2},\qquad Pr=\frac{\nu}{a}$$
$$Ra=Gr\,Pr,\qquad Ra^*=Ra(b/L_h) \tag{5}$$

Eqs. (2)–(4) were solved by imposing the boundary conditions shown in Table 1. They are uniform heat flux and no-slip condition on the channel plates; adiabatic wall and no-slip condition on the other solid walls; boundary at ambient temperature and normal component of the velocity gradient equal to zero on the lower reservoir and adiabatic boundary and normal component of the velocity gradient equal to zero on upper reservoir.

The local convective coefficient can be computed with the local Nusselt number, for the heated region as:

$$Nu(X)=\frac{h(x)b}{k}=\frac{1}{\theta_w(X)} \tag{6}$$

The average value can be written as:

$$Nu=\frac{b}{L_h}\int_0^{L_h/b} Nu(X)\,dX \tag{7}$$

In order to evaluate the optimal geometrical configurations in terms of expansion ratio $B/b$, dimensionless parameters, such as average Nusselt number, dimensionless maximum wall temperature and mass flow rate are referred to the correspondent values for simple channel $Nu_0$, $\theta_{w,\max 0}$ and $\Delta\Psi_0$. The optimal $B/b$ values are graphically evaluated where the maximum values of $Nu/Nu_0$ and $\Delta\Psi/\Delta\Psi_0$ or the minimum $\theta_{w,\max}/\theta_{w,\max 0}$ are attained. The dependences of the three ratios, $Nu/Nu_0$, $\Delta\Psi/\Delta\Psi_0$ and $\theta_{w,\max}/\theta_{w,\max 0}$ are in terms of $Ra^*$, $B/b$ and $L/L_h$. For assigned $Ra^*$ and $L/L_h$ the existence of the optimal geometrical configuration is established in [8,18,22]. The values of the three ratios are evaluated with the numerical model here proposed. This similar procedure was employed in many investigations and it is very useful in complex geometries in natural and forced convection [4,5,9,10,18,23–25].

Table 2
Average Nusselt number, $Nu$, and dimensionless mass flow rate, $\Delta\Psi$, as a function of $n_x$ for $n_y=21$ and as a function of $n_y$ for $n_x=71$, for $Ra=10^4$, $L_h/b=10$, $L/L_h=2.0$ and $B/b=2.0$

| $n_y=21$ | | | $n_x=71$ | | |
|---|---|---|---|---|---|
| $n_x$ | $Nu$ | $\Delta\Psi$ | $n_y$ | $Nu$ | $\Delta\Psi$ |
| 35 | 3.796 | 170.0 | 11 | 3.829 | 170.0 |
| 51 | 3.841 | 168.3 | 15 | 3.863 | 168.4 |
| 61 | 3.864 | 168.2 | 19 | 3.878 | 168.2 |
| 71 | 3.883 | 168.1 | 21 | 3.883 | 168.1 |
| 81 | 3.897 | 168.1 | 25 | 3.889 | 168.1 |
| 91 | 3.909 | 168.0 | 27 | 3.891 | 168.0 |
| 111 | 3.927 | 167.9 | | | |

## 3. Numerical scheme

The numerical computation was carried out with the control volume approach, using rectangular cells with constant mesh spacing. The vorticity and energy equations, Eqs. (2), (4), were solved with the Alternating Direction Implicit (ADI) method with the false transient procedure [28]. The second-order upwind scheme [29] was employed to discretize the convective derivatives, whereas the diffusive derivatives were discretized by the classical central three-point scheme. The numerical procedure was described in detail in [18].

Preliminary tests were carried out to verify the accuracy of the numerical solution. Two global variables, $\Delta\Psi$ and $Nu$, were monitored to analyze the numerical solution independence of the mesh spacing, as reported in [18] and shown in Table 2. The $\Delta\Psi$ represents the induced mass flow rate through the channel and, in dimensionless terms, under the hypothesis of incompressible flow, the mass flow rate $\Delta\Psi$ is coincident with the volumetric flow rate. In the table, $n_x$ is the number of nodes in the channel along $x$-direction and $n_y$ is the number of nodes in the channel along $y$-direction. By means of this analysis a $71\times 21$ grid inside the channel ensured a good compromise between the machine computational time and the accuracy requirements. For the chimney and the two reservoirs, a grid with the same constant cell aspect ratio of the channel has been employed; this choice does not affect the numerical accuracy because in these regions the lowest temperature gradients are present.

Other tests were made to calculate the minimum vertical, $L_x$, and horizontal, $L_y$, reservoir dimensions, which do not alter the dynamic and thermal fields inside the channel with a prescribed accuracy ($10^{-4}$). In the numerical procedure, a vertical reservoirs dimension $L_x$ equal to twice the channel height was employed, whereas a horizontal reservoirs dimension $L_y$ equal to eleven times the channel width, $b$, was chosen.

A comparison between the average Nusselt number obtained experimentally and numerically is shown in Fig. 2. For $Ra=$

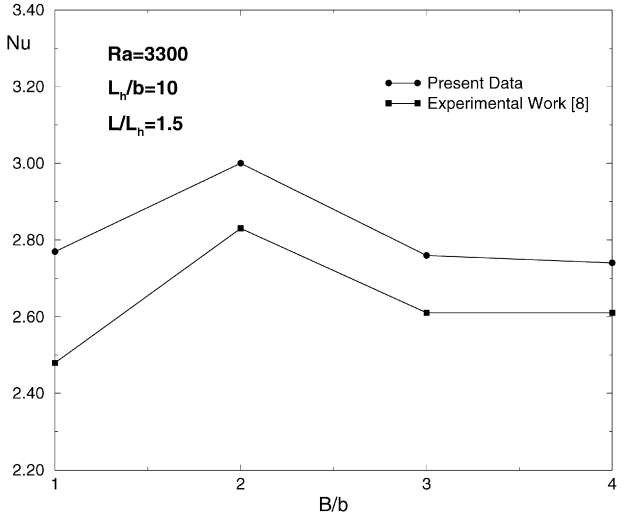


Fig. 2. Comparison between present numerical and experimental [8] average Nusselt numbers: (a) at $Ra = 3300$, for $L_h/b = 10$ and $L/L_h = 1.5$; (b) comparison with correlation given in [8].

3300, $L_h/b = 10$ and $L/L_h = 1.5$, Fig. 2(a), the difference between the numerical results and the experimental ones is less than 12% and their behavior is the same. In Fig. 2(b), a comparison between the numerical average Nusselt number values and an experimental correlation, given in [8], is reported. The correlation is:

$$Nu = \left(\frac{L}{L_h}\right)^{0.268} \left\{ \left[ 0.259 \left( Ra^* \frac{B}{b} \right)^{0.399} \right]^{-2.02} + \left[ 1.42 \left( Ra^* \frac{B}{b} \right)^{0.150} \right]^{-2.02} \right\}^{-1/2.02} \quad (8)$$

Discrepancies between the correlation obtained by means of experimental results and the numerical results are observed. These discrepancies are higher for the lower $Ra^*(B/b)$ values. There is good agreement between the experimental and numerical data and this agreement is as better as the higher the $Ra^*(B/b)$ values and the lower $L/L_h$ values are.

The discrepancies between the numerical and experimental results are due to the conduction phenomenon inside the heated walls of the channel plates present in the experimental study.

## 4. Results and discussion

Results for the parametric analysis are carried out for air, $Pr = 0.71$, in the Rayleigh number range from $10^2$ to $10^5$ and for a channel aspect ratio $L_h/b = 5, 10$ and 20. The expansion ratio, $B/b$, is in the range [1.0–4.0] and the extension ratio, $L/L_h$, ranges from 1.5 to 4.0. No local flow separation around the entrance corner was found in all considered cases.

The analyzed configuration is applied in electronic cooling. Typical geometrical dimensions are referred to $L_h = 100$ mm, with $L - L_h = 0$–300 mm, $b$ is in the range 5.0–40 mm and, consequently, $B$ changes from 5.0 to 160 mm. Heat flux ranges between 3.0 and 500 W/m$^2$. Two actual limit cases are: $b =$ 5.0 mm and a heat flux equal to about 50 W/m$^2$ and the corresponding Rayleigh number is equal to 100 and $b = 40$ mm with a heat flux of about 10 W/m$^2$ and $Ra = 10^5$. The highest considered heat flux, 500 W/m$^2$ and related to $Ra = 10^5$, is attained for $b$ equal to about 15.5 mm.

Wall temperature profiles for $Ra = 10^2$ and $10^5$ and for $L/L_h = 1.5$ and 4.0 are shown in Figs. 3–6 with $L_h/b = 5, 10$ and 20 and for different expansion ratio values. In all cases the highest value of maximum wall temperature is attained for the simple channel configuration. These profiles allow the evaluation of the different thermal behaviors of the channel–chimney system in terms of the channel aspect ratio. In all temperature profiles, the maximum wall temperature is not attained at the channel outlet section but at a slightly lower value of the axial coordinate due to the diffusive effects, according to experimental results given in [8,17,20,21]. The value $X_{\max}$ of the section at which the maximum wall temperature is attained depends on the geometrical parameters and $Ra$ values. In fact, for the simple channel configuration, the point $X_{\max}$ is the lowest among the various configurations for assigned $Ra$ and $L_h/b$, as shown in all Figs. 3–6; this effect is more evident for the lowest $Ra$, in Figs. 3–4. The $X_{\max}$ value, for the same channel length, increases with increasing $L_h/b$ value because the decreasing diffusive effects toward the external ambient. Moreover, increasing the Rayleigh number, the $X_{\max}$ value increases because of the decreasing diffusive effects, as it is noted comparing Fig. 3 with Fig. 5 and Fig. 4 with Fig. 6. A sharp decrease of wall temperature in the outlet section zone is present due to also the cold inflow inside the chimney, which reaches the outlet section of the channel.

For the lowest Rayleigh number, $Ra = 10^2$, and $L/L_h = 1.5$, Fig. 3, wall temperatures decrease with increasing expansion ratio up to $B/b$ between 2.0 and 3.0 and, for higher $B/b$ values, wall temperatures increase again. Moreover, the decrease in the wall temperature at the outlet region for $B/b \leqslant 3.0$ is lower than the one for the simple channel. For $B/b = 4.0$, this decrease is almost equal to the one for the simple channel due to a cold inflow from the outlet section of the chimney. The cold inflow in the chimney was observed in [8,15,17–21] and a fluid stream flows down along the adiabatic extensions. It reaches the

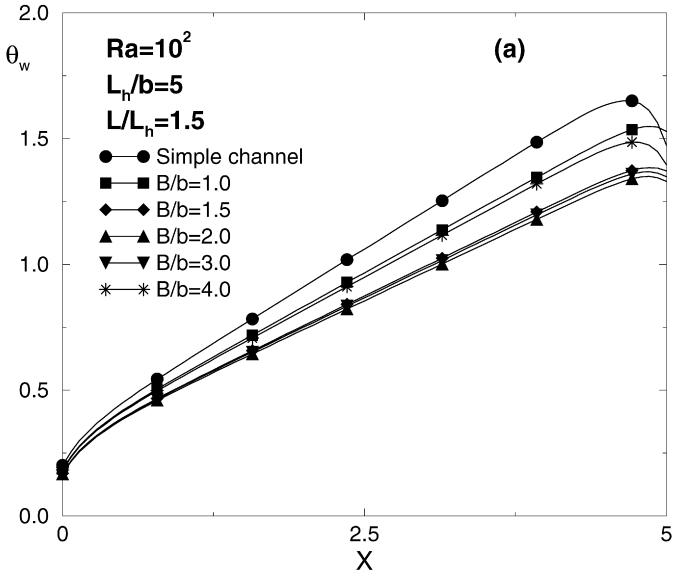


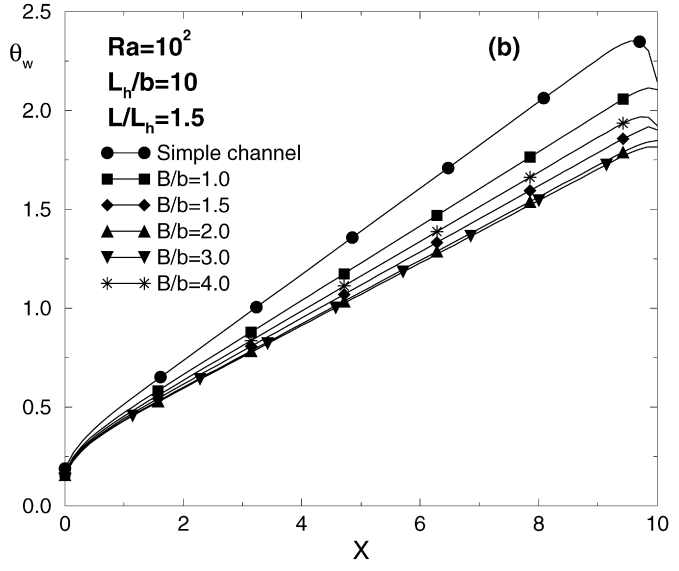


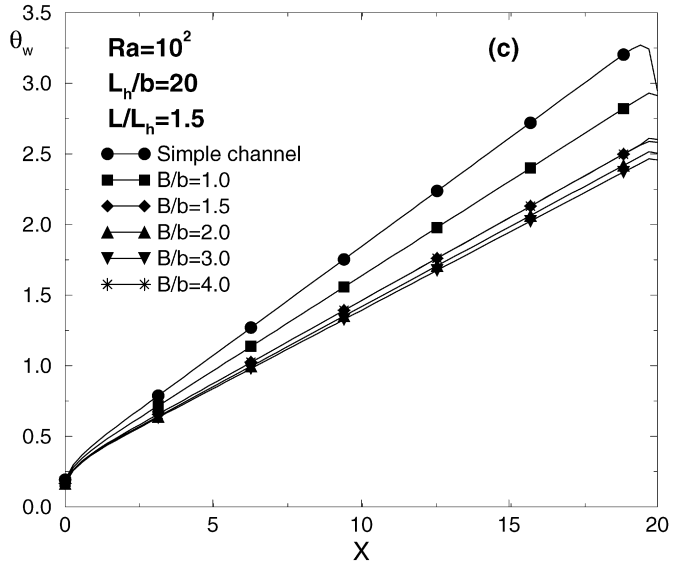


Fig. 3. Heated wall temperatures at $Ra = 10^2$ and $L/L_h = 1.5$ for different channel aspect ratios: (a) $L_h/b = 5$; (b) $L_h/b = 10$ and (c) $L_h/b = 20$.

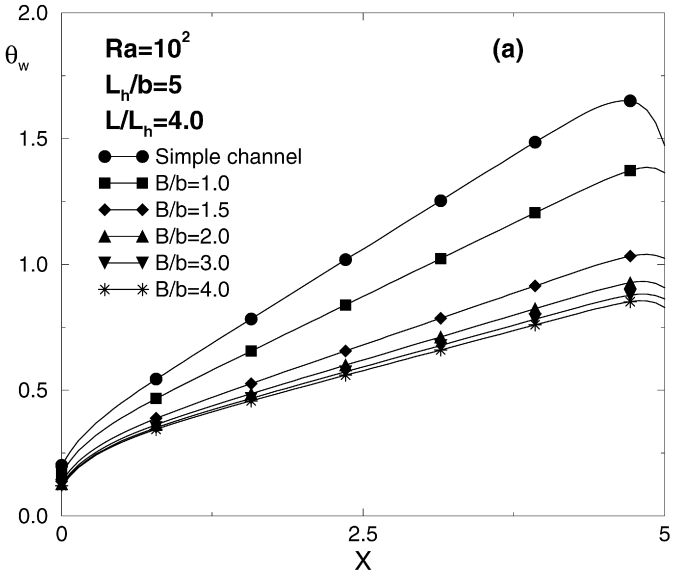


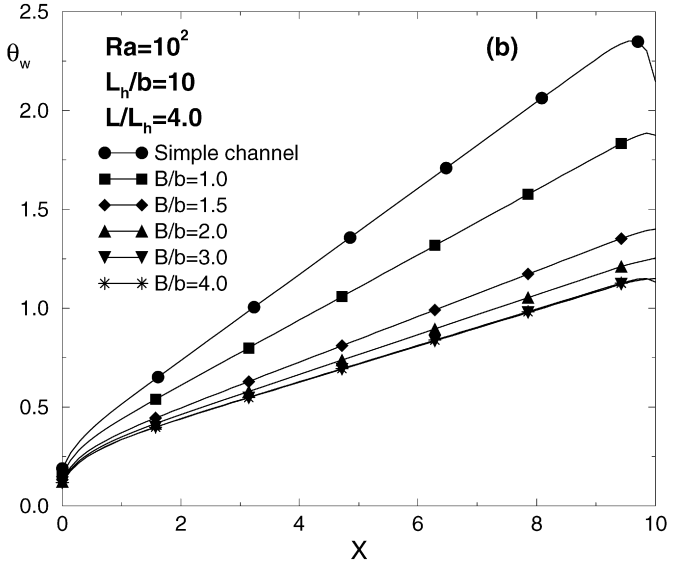


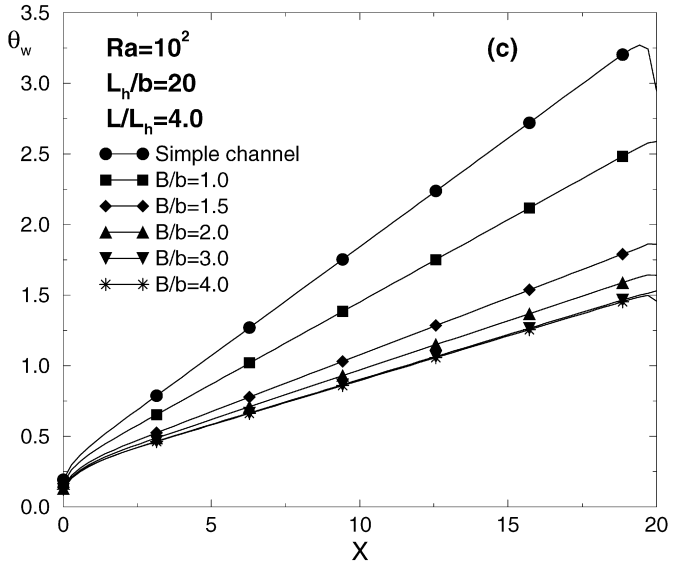


Fig. 4. Heated wall temperatures at $Ra = 10^2$ and $L/L_h = 4.0$ for different channel aspect ratios: (a) $L_h/b = 5$; (b) $L_h/b = 10$ and (c) $L_h/b = 20$.

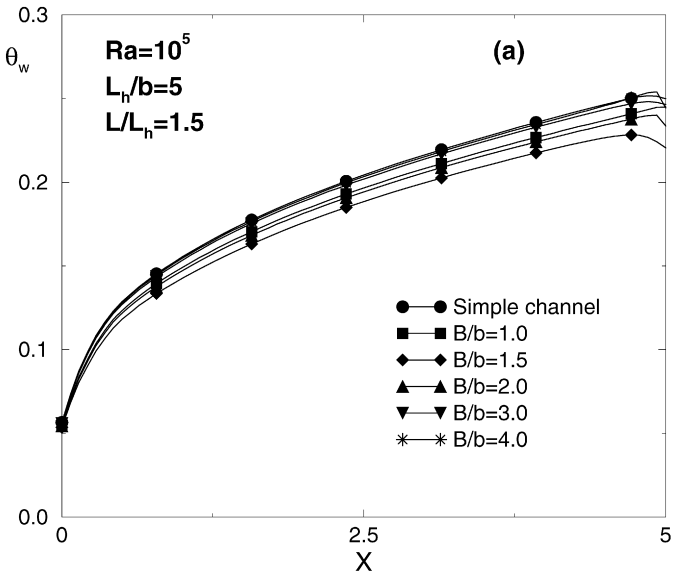


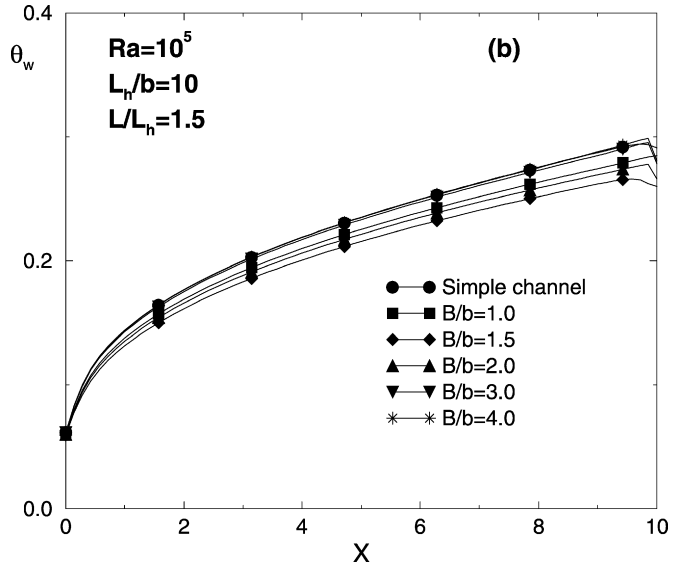


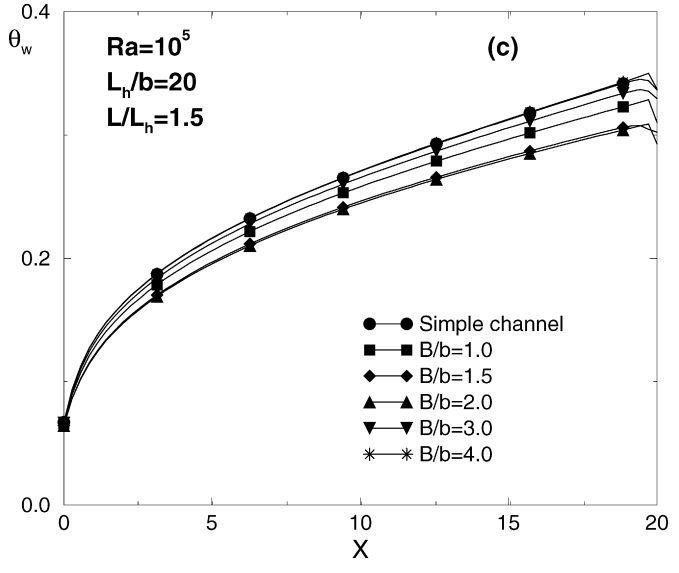


Fig. 5. Heated wall temperatures at $Ra = 10^5$ and $L/L_h = 1.5$ for different channel aspect ratios: (a) $L_h/b = 5$; (b) $L_h/b = 10$ and (c) $L_h/b = 20$.

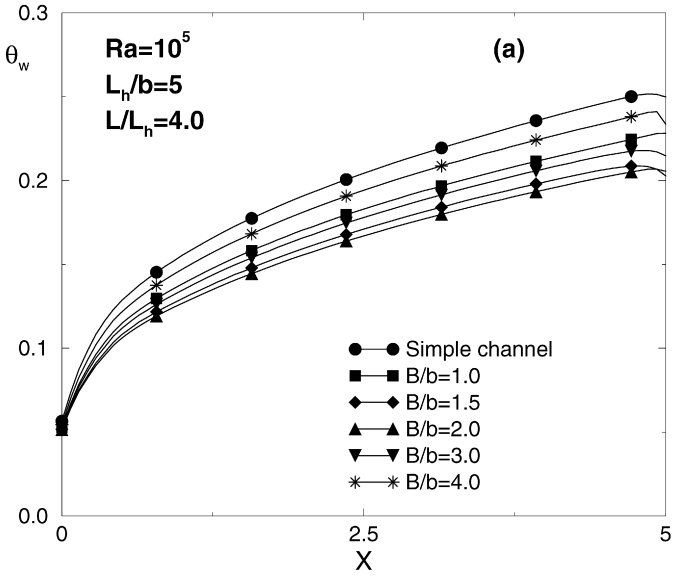


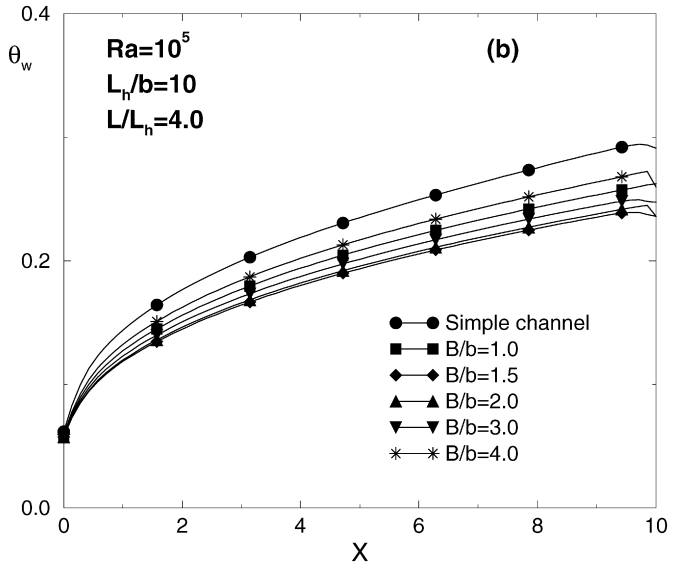


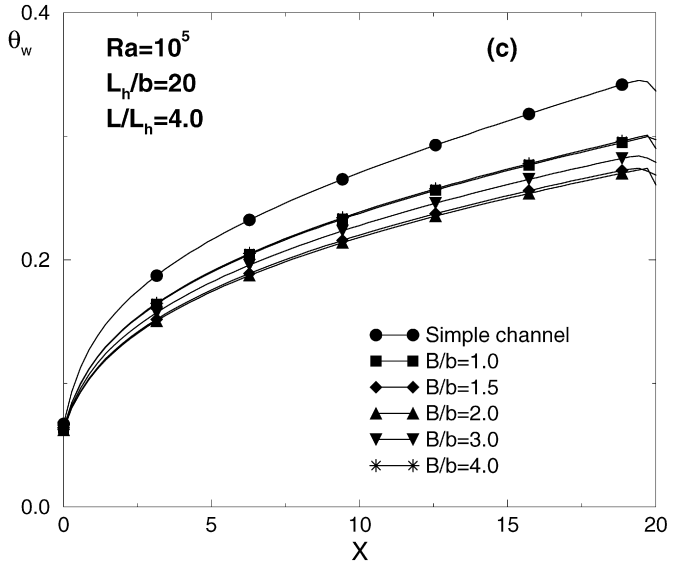


Fig. 6. Heated wall temperatures at $Ra = 10^5$ and $L/L_h = 4.0$ for different channel aspect ratios: (a) $L_h/b = 5$; (b) $L_h/b = 10$ and (c) $L_h/b = 20$.

horizontal wall of the chimney, mixes with the hot plume-jet and goes out of the channel. A consequence of the cold inflow or downflow is a reduction of chimney effect, which gets stronger increasing aspect ratio as indicated in Fig. 3 (b) and (c). The evaluation of cold inflow or downflow has been obtained, following the analysis proposed by Modi and Torrance [30], estimating the position along the adiabatic wall of the chimney where the vorticity goes to 0. As general result, it is observed that the number of configurations with a complete downflow increases at increasing $Ra$ value whereas the number of configurations with a partial separation from the wall decreases. The separation is present for $B/b = 2.0$ only when $L/L_h$ is equal to 1.5 at $Ra \leqslant 10^4$ whereas, for $Ra = 10^5$, only a complete downflow is observed. Some possible guidelines to evaluate critical conditions related to the beginning of flow separation and complete downflow will be provided by means Figs. 7–11. In fact, after the optimal conditions, thermal and fluid dynamics trends indicate a worsening of the chimney effect. However, this investigation, although obtained for steady state, is in agreement with what was suggested in the numerical analysis carried out in [30], but it is remarked that a complete description of the cold inflow or downflow is not possible due to the unsteady nature of this phenomenon, as observed in [30,31].

The difference between the maximum values of the wall temperature for the simple channel and for $B/b = 2.0$ increases with increasing $L_h/b$, just as the increasing difference between the maximum values of the wall temperature for the simple channel and for $B/b = 4.0$. It is possible to affirm that increasing $L_h/b$ allows to enhance the channel–chimney system heat transfer with respect to the simple channel, particularly for the configurations with $B/b > 1.5$.

For $L/L_h = 4.0$, Fig. 4, the absolute differences strongly increase with respect to the previous case ($L/L_h = 1.5$) and this shows that the chimney effect remarkably improves. Moreover, these differences increase with increasing the channel aspect ratio, $L_h/b$. The configuration with $B/b = 4.0$ shows the lowest wall temperature values, but it has to be underlined that the decrease of the maximum wall temperature is significant even for $B/b$ =1.5, whereas the reduction from the configuration with $B/b = 1.5$ to the configuration with $B/b = 4.0$ is reasonably lower. In fact, the percentage variations of the maximum wall temperature between the configuration with $B/b = 1.5$ and the simple channel, in reference to the value pertinent to the configuration with $B/b = 1.5$, is almost 60%, whereas the variation between the configuration with $B/b = 4.0$ and the one with $B/b = 1.5$ is almost 19% for $L_h/b = 5$. Therefore increasing the channel aspect ratio enhances the thermal behavior of the channel–chimney system for both low $L/L_h$ values and large $L/L_h$ values, for low Rayleigh number values.

For the largest Rayleigh number value here considered, $Ra = 10^5$, Figs. 5 and 6, the wall temperatures are lower than those for the configurations pertinent to $Ra = 10^2$. For $L/L_h = 1.5$, Fig. 5, the configuration with $B/b = 1.5$ shows the lowest maximum wall temperature values, whereas the configuration with $B/b = 4.0$ has wall temperature values similar to the ones pertinent to the simple channel, for all the analyzed $L_h/b$ values. In this configuration the downflow is already present for

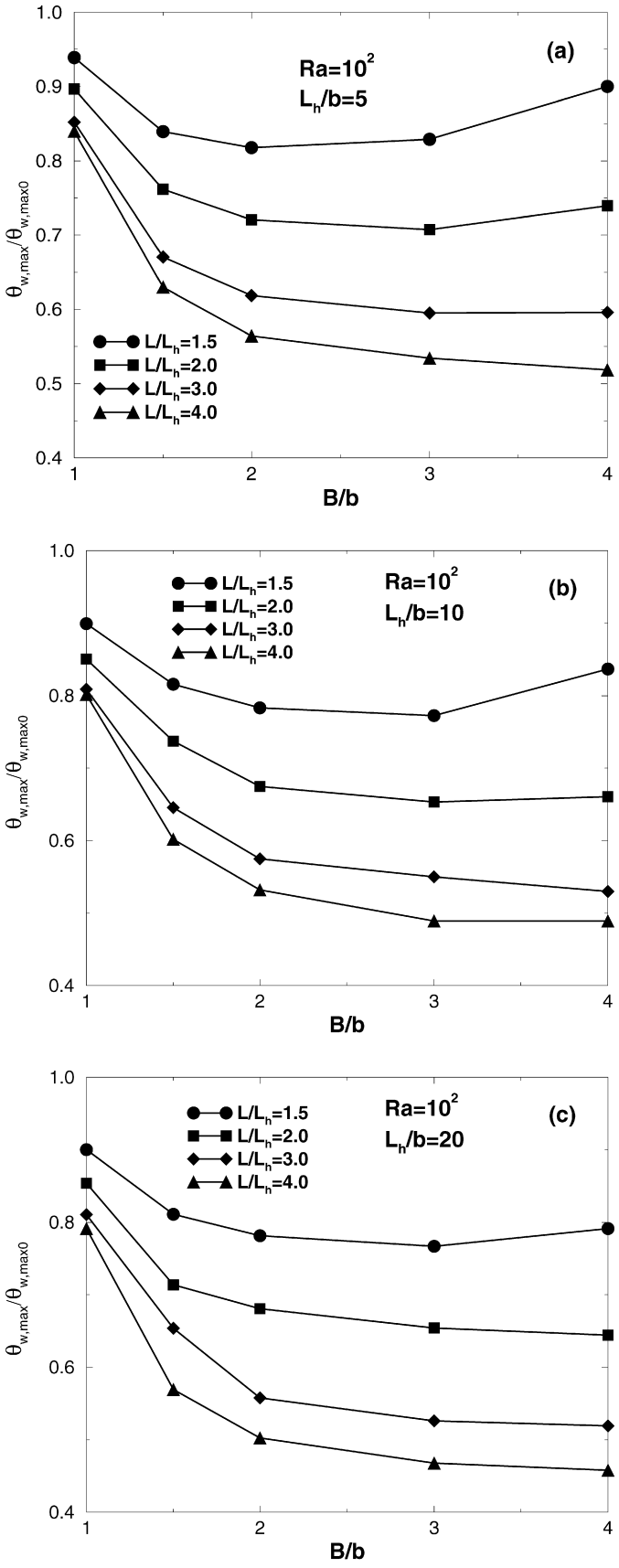


Fig. 7. Ratio of the maximum wall temperature to the simple channel one vs. $B/b$ for different extension ratio values at $Ra = 10^2$: (a) $L_h/b = 5$; (b) $L_h/b = 10$ and (c) $L_h/b = 20$.

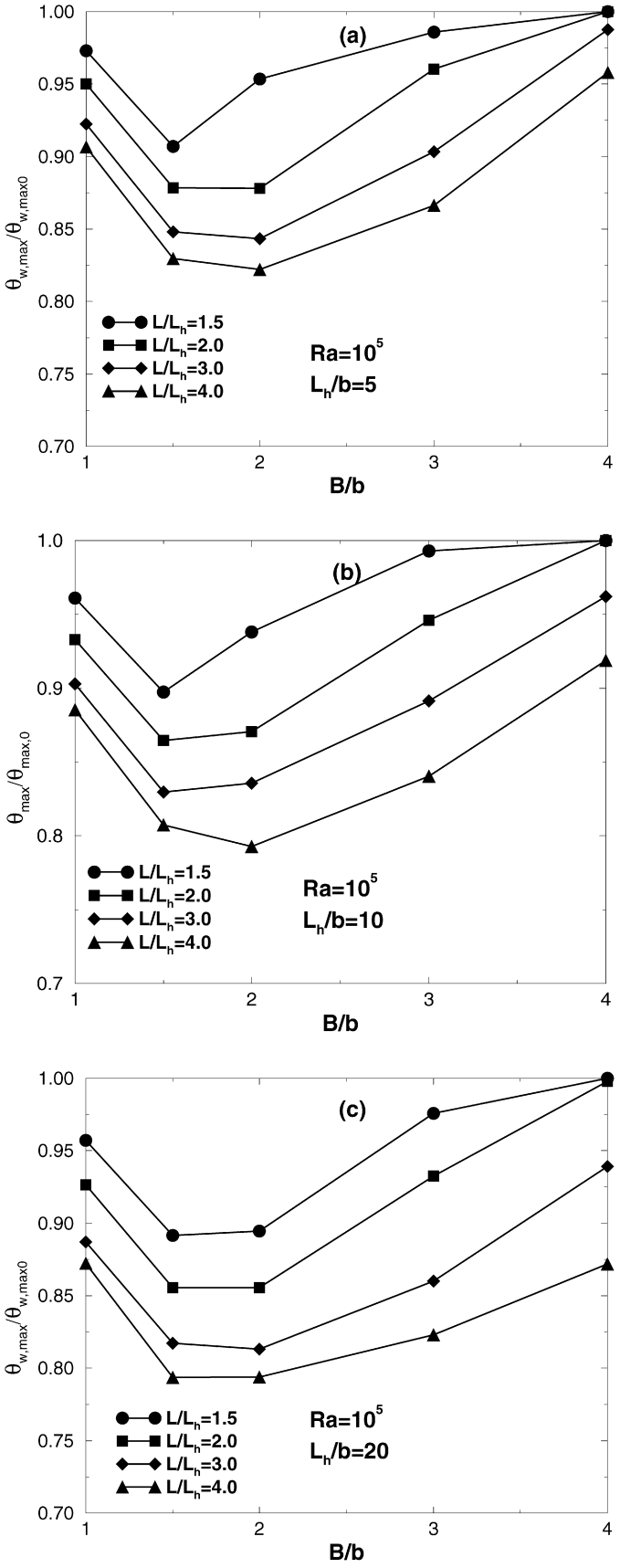


Fig. 8. Ratio of the maximum wall temperature to the simple channel one vs. $B/b$ for different extension ratio values at $Ra = 10^5$: (a) $L_h/b = 5$; (b) $L_h/b = 10$ and (c) $L_h/b = 20$.

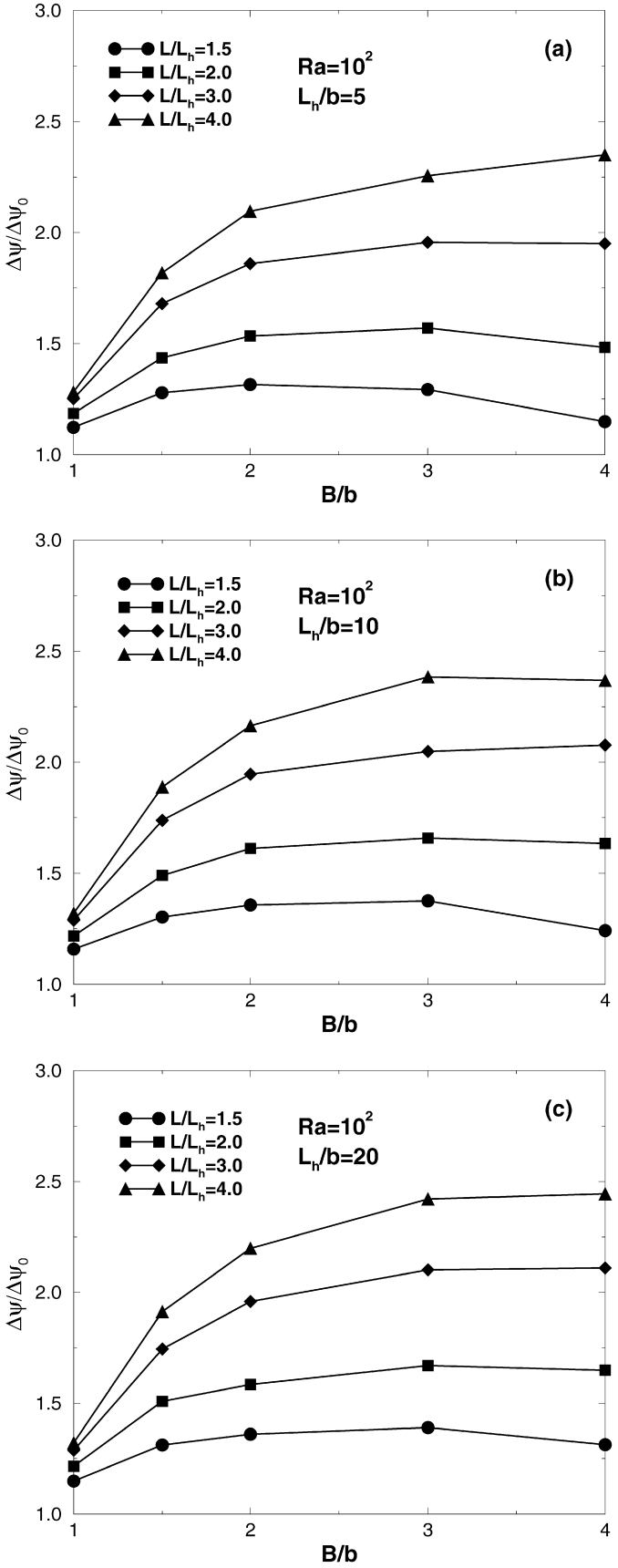


Fig. 9. Ratio of the dimensionless mass flow rate to the simple channel one vs. $B/b$ for different extension ratio values at $Ra = 10^2$: (a) $L_h/b = 5$; (b) $L_h/b = 10$ and (c) $L_h/b = 20$.

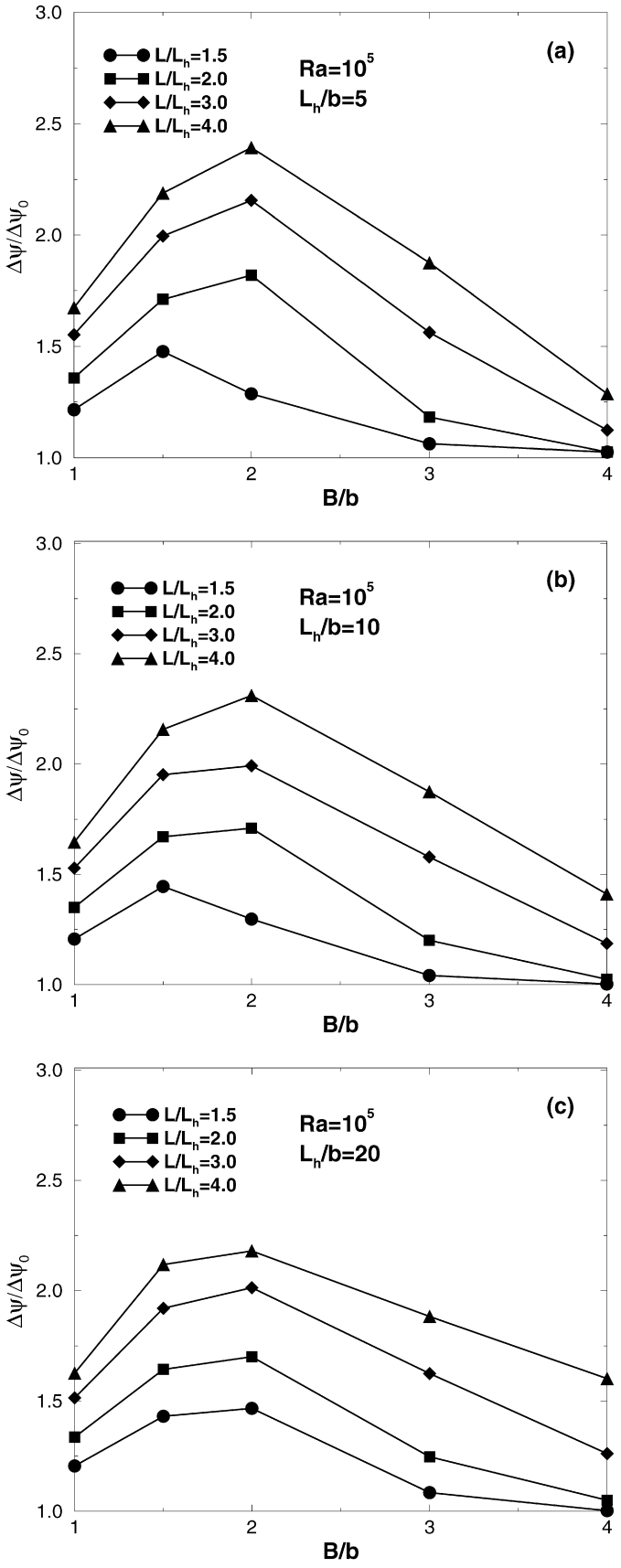


Fig. 10. Ratio of the dimensionless mass flow rate to the simple channel one vs. $B/b$ for different extension ratio values at $Ra = 10^5$: (a) $L_h/b = 5$; (b) $L_h/b = 10$ and (c) $L_h/b = 20$.

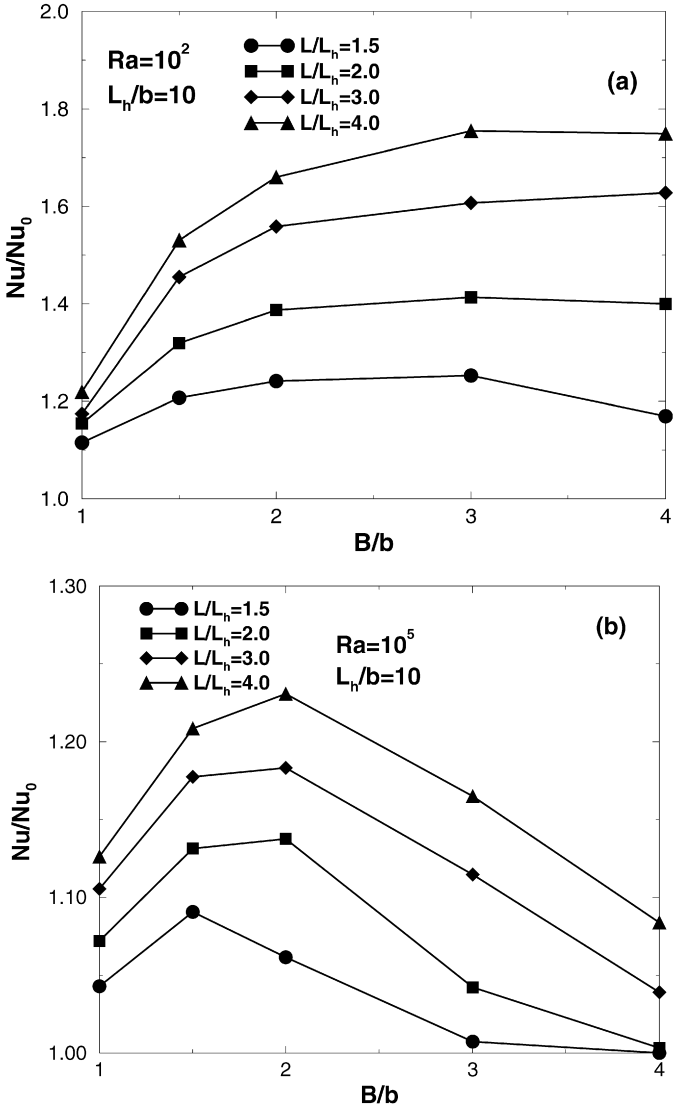


Fig. 11. Ratio of the average Nusselt number to the simple channel one vs. $B/b$ for different extension ratio values and $L_h/b = 10$: (a) $Ra = 10^2$; (b) $Ra = 10^5$.

$B/b = 2.0$. This is due to the larger velocity of the hot jet coming out the channel, which determines the fluid separation from the adiabatic chimney wall. Also in this case, the $L_h/b$ increase produces an enhancement of the channel–chimney system with respect to the simple channel, as observed in Fig. 5.

For $Ra = 10^5$ and $L/L_h = 4.0$, Fig. 6, the lowest wall temperatures are obtained for $B/b = 2.0$. This shows that, by also increasing the chimney height remarkably, the cold inflow is present, causing a decrease in the chimney effect. In fact, for $L_h/b = 5$, Fig. 6(a), it is observed that the wall temperature decreases up to $B/b = 2.0$ and then it increases again for $B/b \geqslant 3.0$. For the highest analyzed $L_h/b$ values, Fig. 6 (b) and (c), it is observed that the difference between the wall temperature values for $B/b = 2.0$ and the ones for the simple channel increases. An increase in the chimney effect, when the channel aspect ratio increases, for the highest Rayleigh number for all the analyzed $L/L_h$ values, is also present. For $Ra = 10^5$ the cold inflow determines optimal configurations for $B/b \leqslant 2.0$ for the highest extension ratio.

To obtain quantitative values and furnish a better analysis of the thermal behavior of the system, the values of the ratio $\theta_{w,\max}/\theta_{w,\max 0}$ between the maximum temperature of the channel–chimney system and the one of the simple channel as a function of the expansion ratio are reported in Figs. 7 and 8, for $L/L_h$ from 1.5 to 4.0.

At $Ra = 10^2$, Fig. 7, the ratio $\theta_{w,\max}/\theta_{w,\max 0}$ is less than 1 for all the analyzed configurations. In agreement with the wall temperature profiles, the ratio decreases, attaining a minimum value, and then it increases for $L/L_h = 1.5$ for all $L_h/b$ values, whereas for $L_h/b = 5$ the ratio $\theta_{w,\max}/\theta_{w,\max 0}$ attains a minimum value as well as for the configuration with $L/L_h = 2.0$, as observed in Fig. 7(a). For the other analyzed $L/L_h$ values the ratio $\theta_{w,\max}/\theta_{w,\max 0}$ profile does not show a minimum or a maximum value in the considered interval. It is interesting to observe that the difference between the ratio $\theta_{w,\max}/\theta_{w,\max 0}$ for $L/L_h = 1.5$ and that for $L/L_h = 4.0$ increases when the expansion ratio increases, for a fixed $B/b$ value. In fact, it goes from 0.102 to 0.307. For $L_h/b = 10$, Fig. 7(b), the values of the ratio $\theta_{w,\max}/\theta_{w,\max 0}$ are always lower than the ones corresponding to the configuration with $L_h/b = 5$. Moreover, the differences between the values at $L/L_h = 1.5$ and at $L/L_h = 4.0$ still increase and for $B/b = 1.0$ the value is about 0.105, whereas it is about 0.345 for $B/b = 4.0$. For $L_h/b = 20$ the values are very close to those for $L_h/b = 10$ and the differences are the same.

At $Ra = 10^5$, Fig. 8, the optimal configurations, such as the configurations for which the $\theta_{w,\max}/\theta_{w,\max 0}$ value is minimum, are those with the expansion ratio value, $B/b$, between 1.5 and 2.0 for all the considered extension ratios. Moreover, for $L/L_h = 1.5$ and 2.0, the configuration with $B/b = 4.0$ shows a channel thermal behavior equal to the simple channel one for all the analyzed channel aspect ratio values, the $\theta_{w,\max}/\theta_{w,\max 0}$ ratio being equal to 1.0. This is due to the downflow which is present for these configurations. Moreover, the $\theta_{w,\max}/\theta_{w,\max 0}$ values decrease with increasing $L_h/b$ whereas the differences between the values at $L/L_h = 1.5$ and $L/L_h = 4.0$ increase. In fact, at $B/b = 1.0$, the differences are 0.068 for $L_h/b = 5$, 0.075 for $L_h/b = 10$ and 0.087 for $L_h/b = 20$, whereas at $B/b = 4.0$ they are 0.041, 0.083 and 0.128, respectively.

The values of the ratio $\Delta\Psi/\Delta\Psi_0$ of the mass flow rate of the channel–chimney system on the simple channel system, as a function of the expansion ratio, are reported in Figs. 9 and 10, for $L/L_h$ ranging from 1.5 to 4.0, for $Ra = 10^2$ and $Ra = 10^5$, respectively. The values of the ratio $\Delta\Psi/\Delta\Psi_0$ are always greater than 1.0, showing that the mass flow rate in the channel–chimney system is always greater than the one in the simple channel, except for $Ra = 10^5$ at the lower $L/L_h$ values. In fact, for these configurations at $B/b = 4.0$, $\Delta\Psi/\Delta\Psi_0$ is almost equal to 1.0 for all the $L_h/b$ values. For $Ra = 10^2$, Fig. 9, it is observed that the mass flow rate, pertinent to the channel–chimney system, is about two and half times that pertinent to the simple channel when $B/b \geqslant 3.0$ for $L/L_h = 4.0$ and for all $L_h/b$ values. The differences between the $\Delta\Psi/\Delta\Psi_0$ ratios for $B/b = 1.0$ for the different analyzed extension ratios are far lower than the same differences for $B/b = 4.0$. This shows that, for a fixed and low extension ratio, the increase in the expansion ratio produces variations significantly lower than those pertinent to the higher $L/L_h$ values. In most configurations with a fixed $L/L_h$ value, the maximum values of $\Delta\Psi/\Delta\Psi_0$ are present for $B/b$ in the range [1.5–4.0].

For $Ra = 10^5$, in Fig. 10, the maximum values of $\Delta\Psi/\Delta\Psi_0$ ratio are always obtained for $B/b \leqslant 2.0$ and they depend on $L_h/b$ more significantly than for $Ra = 10^2$, especially when $L/L_h = 3.0$ and $L/L_h = 4.0$. These results confirm the chimney effect worsening for the channel–chimney system when the downflow is present in the chimney and they allow for a quantitative evaluation of the decrease in the mass flow rate. Moreover, comparing the configurations for $Ra = 10^2$, Fig. 9, with those for $Ra = 10^5$, Fig. 10, it is observed that, for $B/b = 1.0$, increase in $L/L_h$ determines a larger increase in $\Delta\Psi/\Delta\Psi_0$ ratio for $Ra = 10^5$ for all the analyzed $L_h/b$ values.

Analogous trends are obtained for the $Nu/Nu_0$ ratio, where $Nu$ is the average Nusselt number pertinent to the channel–chimney system and $Nu_0$ is the one pertinent to the simple channel. The values of the ratio $Nu/Nu_0$ as a function of the expansion ratio are reported in Figs. 11 (a) and (b), for $L/L_h$ from 1.5 to 4.0 and $L_h/b = 10$, for $Ra = 10^2$ and $Ra = 10^5$, respectively. The trends and the dependence on $L_h/b$ are qualitatively very similar to those shown in Figs. 9 and 10 whereas the differences are strong between the ratios pertinent to $Ra = 10^2$, in Fig. 11(a), and to $Ra = 10^5$, in Fig. 11(b). In fact, for $Ra = 10^2$, $Nu/Nu_0$ reaches a maximum value of about 1.8, whereas for $Ra = 10^5$ the maximum value is slightly higher than 1.2. This indicates that, for the lowest considered $Ra$ value, the heat transfer enhances more significantly in the channel–chimney system, whereas, for the highest considered $Ra$ value, the heat transfer enhancement due to the employment of chimney is larger than 20% with respect to the simple channel. The maximum wall temperature, average Nusselt number and mass flow rate ratio, for smaller $L/L_h$, present their minimum and maximum value, respectively, at $B/b = 1.5$ and, for higher $B/b$ value, $\theta_{w,\max}/\theta_{w,\max 0}$ increases and $Nu/Nu_0$ and $\Delta\Psi/\Delta\Psi_0$ decrease due to the cold inflow presence, which determines a decrease of the chimney effect. For $L/L_h > 1.5$, the cold inflow starts at higher $B/b$ value and, at $B/b = 2.0$, $\theta_{w,\max}/\theta_{w,\max 0}$ attains the minimum value whereas $Nu/Nu_0$ and $\Delta\Psi/\Delta\Psi_0$ present the maximum value.

This observation is more evident in Fig. 12, where the maximum values of the ratio $Nu/Nu_0$ are reported for different $L/L_h$, $Ra$ and $L_h/b$ values. For $L_h/b = 20$, there is always an enhancement of a thermal behavior of the system and the ratio $(Nu/Nu_0)_{\max}$ increases when $L/L_h$ increases. For $Ra = 10^2$, with $L/L_h$ passing from 1.5 to 4.0 value, the percentage increase of the ratio $(Nu/Nu_0)_{\max}$ is about 40–45%, whereas for $Ra = 10^5$ it is about 12%.

In the following, correlations of the dimensionless mass flow rate, the dimensionless maximum wall temperature and the average Nusselt number as a function of the channel Rayleigh number and of the expansion and extension ratios are reported. Correlations are in the form: $f(Ra^* B/b, B/b, L/L_h)$. In particular, for the mass flow rate, the following equation is proposed:

$$\Delta\Psi = 3.590 Ra^{0.2323} \left(\frac{L_h}{b}\right)^{0.7323} \left(\frac{B}{b}\right)^{-0.2677} \left(\frac{L}{L_h}\right)^{0.4823} \quad (9)$$

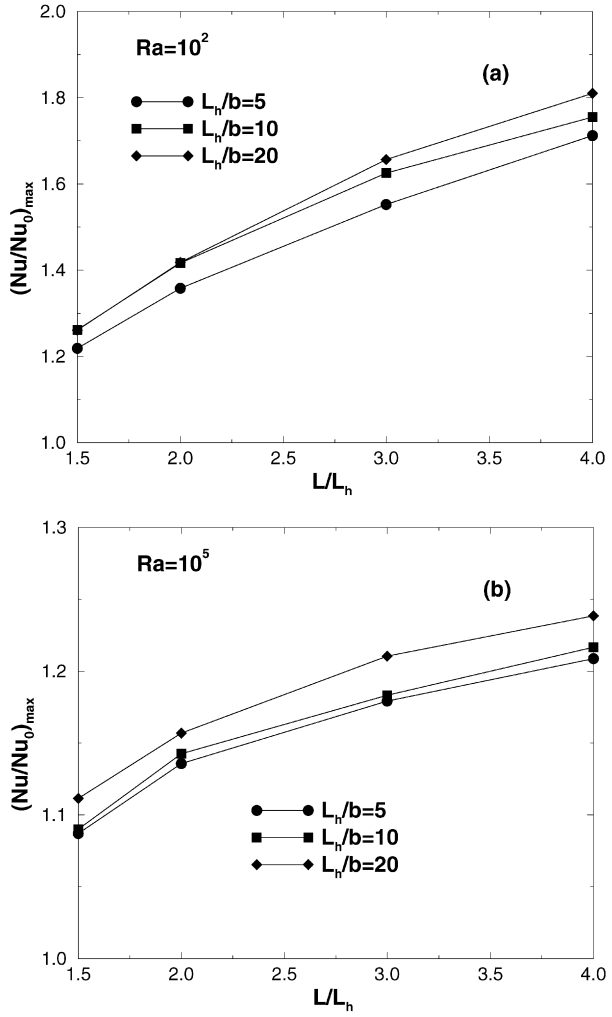


Fig. 12. Maximum values of $Nu/Nu_0$ vs. $L/L_h$ for different $L_h/b$ and $Ra$ values: (a) $Ra = 10^2$; (b) $Ra = 10^5$.

with $r^2 = 0.977$ in the ranges: $5 \leqslant Ra^* \leqslant 2.0 \times 10^4$, $1.5 \leqslant L/L_h \leqslant 4.0$ and $1.0 \leqslant B/b \leqslant 4.0$.

For the average Nusselt number, the following equation is proposed:

$$Nu = \left(\frac{B}{b}\right)^{-0.250}\left(\frac{L}{L_h}\right)^{0.150}\left\{\left[0.570\left(Ra^*\frac{B}{b}\right)^{0.306}\right]^{-11} + \left[1.155\left(Ra^*\frac{B}{b}\right)^{0.161}\right]^{-11}\right\}^{-1/11} \quad (10)$$

with $r^2 = 0.984$ in the ranges: $5 \leqslant Ra^* \leqslant 2.0 \times 10^4$, $1.5 \leqslant L/L_h \leqslant 4.0$ and $1.0 \leqslant B/b \leqslant 4.0$. It is interesting to observe that the average Nusselt number increases when $L/L_h$ increases, even if it is raised to the power of 0.150.

For the dimensionless maximum wall temperature the following equation is proposed:

$$\theta_{w,\max} = \left(\frac{B}{b}\right)^{0.250}\left(\frac{L}{L_h}\right)^{-0.30}\left\{\left[2.02\left(Ra^*\frac{B}{b}\right)^{-0.199}\right]^{1.30} + \left[8.79\left(Ra^*\frac{B}{b}\right)^{-0.757}\right]^{1.30}\right\}^{1/1.30} \quad (11)$$

with $r^2 = 0.983$ in the ranges: $5 \leqslant Ra^* \leqslant 2.0 \times 10^4$, $1.5 \leqslant L/L_h \leqslant 4.0$ and $1.0 \leqslant B/b \leqslant 4.0$. The $\theta_{w,\max}$ variations, with respect to the considered independent variables, are the inverse of those pertinent to $Nu$.

The values of optimal expansion ratio $(B/b)_{\text{opt}}$, for each analyzed extension ratio, are evaluated. These values correspond to the minimum value of the $\theta_{w,\max}/\theta_{w,\max 0}$ ratio for all the considered $Ra$ values. The following correlation is obtained:

$$\left(\frac{B}{b}\right)_{\text{opt}} = 2.13(Ra^*)^{-0.065}\left(\frac{L}{L_h}\right)^{0.468} \quad (12)$$

with $r^2 = 0.984$ in the ranges: $5 \leqslant Ra^* \leqslant 2.0 \times 10^4$ and $1.5 \leqslant L/L_h \leqslant 4.0$. The $(B/b)_{\text{opt}}$ value increases with increasing $L/L_h$ and it decreases when $Ra^*$ is slightly decreased.

## 5. Conclusions

A parametric study on a channel–chimney system was accomplished in this numerical investigation in order to evaluate some geometric optimal configurations in terms of significant dimensionless geometric and thermal parameters. In the system, the channel walls are symmetrically heated at uniform heat flux.

Temperature wall profiles, as a function of axial coordinate, suggested the evaluation of thermal performances of the channel–chimney system in terms of maximum wall temperatures for different expansion ratios, as a function of the channel aspect ratio. For considered Rayleigh number values, the difference between the highest and the lowest maximum wall temperatures increased with increasing channel aspect ratio. This behavior was as greater as the extension ratio was. These differences decreased significantly for the highest Rayleigh number value. Optimal configurations for assigned $L/L_h$ and $L_h/b$ were evaluated in terms of $B/b$ corresponding to the minimum value of maximum wall temperatures. The optimal $B/b$ values depended strongly on $Ra$ and $L/L_h$ values and slightly on the channel aspect ratio. A more significant increase of maximum average Nusselt number referred to the simple channel value was obtained for the lowest considered $Ra$ value, $Ra = 10^2$, $L_h/b = 20$ and $L/L_h = 4.0$ and it was about 80%, whereas for $Ra = 10^5$ this increase was about 24% for the same $L_h/b$ and $L/L_h$ values.

Correlations for dimensionless mass flow rate, maximum wall temperature and average Nusselt numbers, in terms of Rayleigh number and dimensionless geometrical parameters, were proposed in the following ranges: $10^2 \leqslant Ra \leqslant 10^5$, $1.0 \leqslant B/b \leqslant 4.0$, $1.5 \leqslant L/L_h \leqslant 4.0$ and $5 \leqslant L_h/b \leqslant 20$. Also a correlation for $(B/b)_{\text{opt}}$ in terms of $Ra$, $L/L_h$ and $L_h/b$ was given in the same intervals.

## Acknowledgements

This research is supported by Seconda Università degli Studi di Napoli and Regione Campania with a Legge 5 2005 research grant.

## References


[1] B. Gebhart, Y. Jaluria, R. Mahajan, B. Sammakia, Buoyancy-Induced Flows and Transport, Hemisphere Publ. Corp., Washington, 1988.

[2] O. Manca, B. Morrone, S. Nardini, V. Naso, Natural Convection in Open Channels, in: B. Sunden, G. Comini (Eds.), Computational Analysis of Convection Heat Transfer, WIT Press, Southampton, UK, 2000, pp. 235–278.

[3] S.J. Kim, S.W. Lee, Air Cooling Technology for Electronic Equipment, CRC Press, Boca Raton, FL, 1996.

[4] A. Bejan, Shape and Structure from Engineering to Nature, Cambridge University Press, New York, 2000.

[5] G.A. Ledezma, A. Bejan, Optimal geometric arrangement of staggered vertical plates in natural convection, ASME J. Heat Transfer 119 (1997) 700–708.

[6] S. Sathe, B. Sammakia, A review of recent developments in some practical aspects of air-cooled electronic packages, ASME J. Heat Transfer 120 (1998) 830–839.

[7] A. Bejan, A.K. da Silva, S. Lorente, Maximal heat transfer density in vertical morphing channels with natural convection, Numer. Heat Transfer A 45 (2004) 135–152.

[8] A. Auletta, O. Manca, B. Morrone, V. Naso, Heat transfer enhancement by the chimney effect in a vertical isoflux channel, Int. J. Heat Mass Transfer 44 (2001) 4345–4357.

[9] A.K. da Silva, L. Gosselin, Optimal geometry of L- and C-shaped channels for maximum heat transfer rate in natural convection, Int. J. Heat Mass Transfer 48 (2005) 609–620.

[10] A. Andreozzi, A. Campo, O. Manca, Compounded natural convection enhancement in a vertical parallel-plate channel, Int. J. Thermal Sciences 47 (6) (2008) 742–748.

[11] S.E. Haaland, E.M. Sparrow, Solutions for the channel plume and the parallel-walled chimney, Numer. Heat Transfer 6 (1983) 155–172.

[12] P.H. Oosthuizen, A numerical study of laminar free convective flow through a vertical open partially heated plane duct, ASME HTD—Fundamentals of Natural Convection—Electronic Equipment Cooling 32 (1984) 41–48.

[13] K.T. Lee, Natural convection in vertical parallel plates with an unheated entry or unheated exit, Numer. Heat Transfer A 25 (1994) 477–493.

[14] A. Campo, O. Manca, B. Morrone, Numerical analysis of partially heated vertical parallel plates in natural convective cooling, Numer. Heat Transfer A 36 (1999) 129–151.

[15] Y. Asako, H. Nakamura, M. Faghri, Natural convection in a vertical heated tube attached to a thermally insulated chimney of a different diameter, ASME J. Heat Transfer 112 (1990) 790–795.

[16] A.G. Straatman, J.D. Tarasuk, J.M. Floryan, Heat transfer enhancement from a vertical, isothermal channel generated by the chimney effect, ASME J. Heat Transfer 115 (1993) 395–402.

[17] A. Auletta, O. Manca, Heat and fluid flow resulting from the chimney effect in a symmetrically heated vertical channel with adiabatic extensions, Int. J. Thermal Sciences 41 (2002) 1101–1111.

[18] A. Andreozzi, B. Buonomo, O. Manca, Numerical study of natural convection in vertical channels with adiabatic extensions downstream, Numer. Heat Transfer A 47 (2005) 1–22.

[19] G.A. Shahin, J.M. Floryan, Heat transfer enhancement generated by the chimney effect in systems of vertical channel, ASME J. Heat Transfer 121 (1999) 230–232.

[20] O. Manca, M. Musto, V. Naso, Experimental analysis of asymmetrical isoflux channel–chimney systems, Int. J. Thermal Sciences 42 (2003) 837–846.

[21] O. Manca, M. Musto, V. Naso, Experimental investigation of natural convection in an asymmetrically heated vertical channel with an asymmetric chimney, ASME J. Heat Transfer 127 (2005) 888–896.

[22] A. Auletta, O. Manca, M. Musto, S. Nardini, Thermal design of symmetrically and asymmetrically heated channel–chimney systems in natural convection, Appl. Thermal Engrg. 23 (2003) 605–621.

[23] A. Bejan, Y. Fautrelle, Constructal multi-scale for maximal heat transfer density, Acta Mech. 163 (2003) 39–49.

[24] A.K. da Silva, A. Bejan, Constructal multi-scale structure for maximal heat transfer density in natural convection, Int. J. Heat Fluid Flow 26 (2005) 34–44.

[25] A.K. da Silva, S. Lorente, A. Bejan, Constructal multi-scale structures for maximal heat transfer density, Energy 31 (2006) 620–635.

[26] D.J. Harris, N. Helwig, Solar chimney and building ventilation, Appl. Energy 84 (2007) 135–146.

[27] E. Bacharoudis, M.G. Vrachopoulos, M.K. Koukou, D. Margaris, A.E. Filios, S.A. Mavrommatis, Study of the natural convection phenomena inside a wall solar chimney with one wall adiabatic and one wall under a heat flux, Appl. Thermal Engrg. 27 (2007) 2266–2275.

[28] J.P. Roache, Fundamentals of Computational Fluid Dynamics, Hermosa Publ., Albuquerque, NM, 1998.

[29] K.E. Torrance, Numerical methods in heat transfer, in: W.M. Rohsenow, J.P. Hartnett, Y.I. Cho (Eds.), Handbook of Heat Transfer, third ed., McGraw-Hill, New York, 1998.

[30] V. Modi, K.E. Torrance, Experimental and numerical studies of cold inflow at the exit of buoyant channel flows, J. Heat Transfer 109 (1987) 392–404.

[31] S. Kazansky, V. Dubovsky, G. Ziskind, R. Letan, Chimney-enhanced natural convection from a vertical plate: Experiments and numerical simulations, Int. J. Heat Mass Transfer 46 (2003) 497–512.